Expression of mechanical characteristics in compacted soil with soil/water/air coupled F.E. simulation

Expression des caractéristiques mécaniques des sols compactés par une simulation couplée sol/eau/air par éléments finis

Kawai K., Iizuka A.
Kobe University

Kanazawa S.
Chuo University

ABSTRACT: Results obtained in a lab compaction test are difficult to apply to the design and compaction control at an actual geotechnical engineering site. This is attributed to the fact that the mechanism for compaction has not been explained using the principles of soil mechanics. The main theme of this study is interpretation of the compaction mechanism with unsaturated soil mechanics. Here, static compaction tests were simulated with soil/water/air coupled finite element analysis code DACSAR-MP. Consequently, the shape of the compaction curve was successfully expressed. Moreover, the effects of compaction on compressibility and permeability of compacted soil could be reasonably explained. Additionally, shear deformation was applied to the specimen obtained from static compaction simulations in soil/water/air coupled analysis. The relationships between shear strength and compaction curve showed good agreement with the actual behavior.

Résumé : Les résultats des essais de compactage obtenus dans un laboratoire sont difficilement applicables à la conception et au contrôle de compactage dans des sites géotechniques d'ingénierie réels. Ceci peut être attribué au fait que le mécanisme du compactage n'a pas été expliqué à partir des principes de la mécanique des sols. Le principal thème de cette étude est de définir le mécanisme de compactage en considérant les principes de base de la mécanique des sols non saturés. Dans ce cadre, nous avons simulé le compactage statique avec de la terre, de l'eau ou de l'air doublé d'une analyse par éléments finis, code DACSAR-MP. Ainsi, nous avons pu mettre à jour avec succès la forme de la courbe de compactage. De plus, nous avons réussi à expliquer scientifiquement les effets du compactage sur la compression et la perméabilité des sols compactés. En outre, les essais de cisaillement ont été simulés sur l'éprouvette obtenue à partir de la simulation d'un compactage statique couplée sol/eau/air . Les relations entre la résistance au cisaillement et la courbe de compactage sont parfaitement en accord avec le comportement réel. .

KEYWORDS: Compaction, Unsaturated soil, Soil/water/air coupled simulation

1 INTRODUCTION

Most onshore earth structures, such as the earth dam or embankments and river levees, are constructed by compaction. It is generally known that the maximum dry density appears at the optimum water content under constant compaction load. This relationship is called compaction curve. In previous research, the characteristics of compacted soil were compared with the compaction curve (see Fig. 1). Water content at the extremal values of mechanical characteristics was found to be different from the optimum water content of the compaction curve. This means that increase in dry density does not directly influence increase in shear strength or a decrease in compressibility and permeability. Moreover, in-situ tests (e.g. Proctor: 1933) and/or experimental construction are actually needed for construction of compacted earth structures since compaction effects are dependent on the method of compaction. In this study, the relationship between characteristics of compacted soil and the compaction curve is expressed using soil/water air coupled F. E. Simulation to clarify the compaction mechanism and the characteristics of soil induced by compaction.

2 NUMERICAL MODELS IN SOIL/WATER/AIR COUPLED ANALYSIS

In this study, the soil/water/air coupled F. E. analysis code, known as DACSAR-MP, is used for simulations. The numerical models applied to DACSAR-MP are detailed as follows:

2.1 *Constitutive model for unsaturated soil*

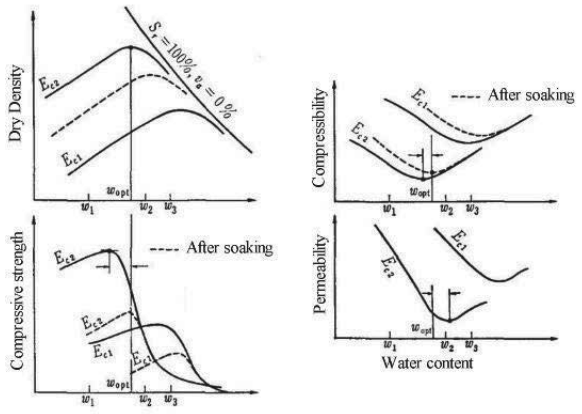

Figure 1. Characteristics of compacted soil with compaction curve (Kuno: 1974)

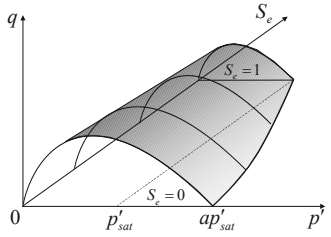

Figure 2. Yield surface of constitutive model for unsaturated soil

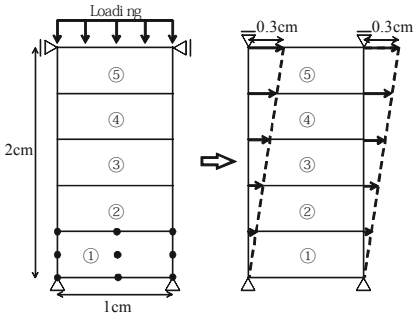

(a) Static compaction (b) Shearing

Figure 3. Analytical mesh and conditions

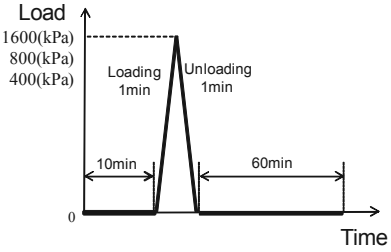

Figure 4. Loading condition

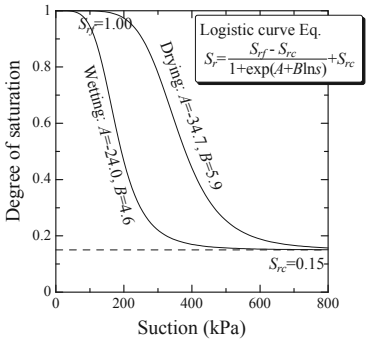

Figure 5. Soil water retention characteristics

Table 1. Material parameters for simulations

λ	κ	k_W (m/day)	M	a	n_s	k_a (m/day)	m
0.107	0.011	0.01	1.344	30	1.0	1.00	0.8

m: Mualem's modulus (1976)

The constitutive model proposed by Ohno et al. (2007) is used. The effective stress for unsaturated soil is defined as;

$$\boldsymbol{\sigma}' = \boldsymbol{\sigma}^{net} + p_s \mathbf{1} \tag{1}$$

$$\boldsymbol{\sigma}^{net} = \boldsymbol{\sigma} - p_a \mathbf{1},\ p_s = S_e s \tag{2}$$

$$s = p_a - p_w,\ S_e = \frac{S_r - S_{rc}}{1 - S_{rc}} \tag{3}$$

Here, $\boldsymbol{\sigma}'$ is the effective stress tensor, $\boldsymbol{\sigma}^{net}$ is the net stress tensor, $\mathbf{1}$ is the unit tensor, $\boldsymbol{\sigma}$ is total stress tensor, s is suction, p_s is suction stress, p_a is pore-air pressure, p_w is pore-water pressure, S_r is degree of saturation, S_e is effective degree of saturation, and S_{rc} is degree of saturation at $s \to \infty$. The yielding function is expressed as;

$$f\left(\boldsymbol{\sigma}', \zeta, \varepsilon_v^p\right) = MD \ln \frac{p'}{\zeta p'_{sat}} + D\frac{q}{p'} - \varepsilon_v^p = 0 \tag{4}$$

$$\zeta = \exp\left[(1 - S_e)^{n_s} \ln a\right],\ MD = \frac{\lambda - \kappa}{1 + e_0} \tag{5}$$

$$p' = \frac{1}{3}\boldsymbol{\sigma}' : \mathbf{1},\ q = \sqrt{\frac{3}{2}\mathbf{s} : \mathbf{s}},\ \mathbf{s} = \boldsymbol{\sigma}' - p'\mathbf{1} = \mathbf{A} : \boldsymbol{\sigma}',\ \mathbf{A} = \mathbf{I} - \frac{1}{3}\mathbf{1} \otimes \mathbf{1} \tag{6}$$

Here, ε_v^p is plastic volumetric strain, M is q/p' in critical state, D is dilatancy coefficient, a and n_s are shape parameters expressing increase in yield stress due to desaturation, and λ and κ are compression and expansion index, respectively. The yield surface expressed by Eq. (4) is illustrated in Figure 2. The following elasto-plastic constitutive model is obtained from Eq.(4) and the associated flow rule.

$$\boldsymbol{\sigma}' = \mathbf{D} : \boldsymbol{\varepsilon} - \mathbf{C} \cdot \dot{S}_e \tag{7}$$

Here, $\mathbf{D}$ is elasto-plastic stiffness matrix, $\boldsymbol{\varepsilon}$ is strain tensor, $\mathbf{C}$ is the tensor expressing change in stiffness due to desaturation.

2.2 *Governing equations of pore-water and pore-air*

The governing equations for pore-water and pore-air are expressed as follows in the track of Borja (2004):

Darcy's law (water) $$\tilde{\mathbf{v}}_\mathbf{w} = -\mathbf{k}_\mathbf{w} \cdot \mathrm{grad} h \tag{8}$$

Darcy's law (air) $$\tilde{\mathbf{v}}_\mathbf{a} = -\mathbf{k}_\mathbf{a} \cdot \mathrm{grad} p_a \tag{9}$$

Continuity equation (water)

$$n\dot{S}_r - S_r \dot{\varepsilon}_v + \mathrm{div}\tilde{\mathbf{v}}_\mathbf{w} = 0 \tag{10}$$

Continuity equation (air)

$$\left(1 - S_r\right)\dot{\varepsilon}_v + n\dot{S}_r - n\left(1 - S_r\right)\frac{\dot{p}_a}{p_a + p_0} - \mathrm{div}\tilde{\mathbf{v}}_\mathbf{a} = 0 \tag{11}$$

Here, $\tilde{\mathbf{v}}_\mathbf{w}$ and $\tilde{\mathbf{v}}_\mathbf{a}$ are flux of pore-water and pore-air, $\mathbf{k}_\mathbf{w}$ and $\mathbf{k}_\mathbf{a}$ are permeability of water and air, h is total head, and p_0 is atmospheric pressure. The formula for the soil/water/air coupled initial and boundary value problems can be obtained by spatially and temporally discretizing Eqs. (7) to (11).

3 ANALYTICAL CONDITIONS

The objective of compaction is compressing soil mass with draining air. In this study, compaction is defined as compression and rebound of unsaturated soil under drained air and undrained water conditions, and the static compaction test is simulated with soil/water air coupled F. E. analysis. Figure 3(a) shows analytical mesh. One-dimensional geometric condition is assumed, and undrained water for all boundaries and drained air for upper boundary conditions are provided. Figure 4 shows the loading condition. Table 1 summarizes the material parameters for simulations and Figure 5 shows soil water retention characteristic curves (SWRCC). The SWRCC model proposed by Kawai et al. (2007) is used here. A void ratio of 0.85 and water content of 10 to 28% are provided for initial conditions. Initial suction is set according to the primary wetting curve. Moreover, shear deformation shown as Figure 3(b) is applied to the specimen obtained from static compaction simulations to examine shear strength of compacted soil (Simple shear simulation).

4 SIMULATION RESULTS AND DISCUSSION

4.1 *Static compaction simulation*

Figure 6 shows changes in the void ratio of element 3 under 800kPa compaction load. The yield stress, the folding point of compression line, is found to depend on water content. Since pore-water is not drained during compaction, the degree of saturation increases with compression due to loading, and the degree of saturation decreases with rebound due to unloading (Figure 7). This behavior is more remarkable on the specimen with higher water content. Figure 8 shows the relationship between suction and the degree of saturation during compaction. According to SWRCC, the increase of saturation due to loading means the wetting process and suction decreases. On the other hand, the decrease of saturation due to unloading creates increase in suction in accordance with the drying process. Consequently, suction changes are more remarkable on the specimen with higher moisture because it shows a relatively bigger change in the degree of saturation (Figure 9). Suction after compaction is greater than before compaction for all specimens. This means that compaction contributes to increase in stiffness of the soil. The specimen with lower moisture shows higher suction after compaction. The changes in pore-air and pore-water pressure are shown in Figures 10 and 11 respectively.

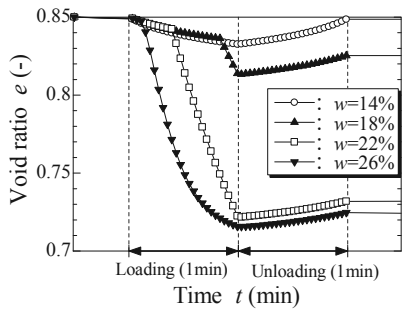

Figure 6. Changes in void ratio of element ○,3

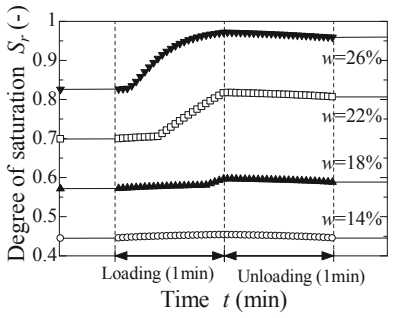

Figure 7. Changes in degree of saturation of element ○,3

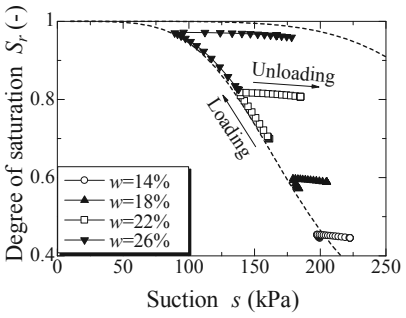

Figure 8. Soil water retention characteristics during compaction

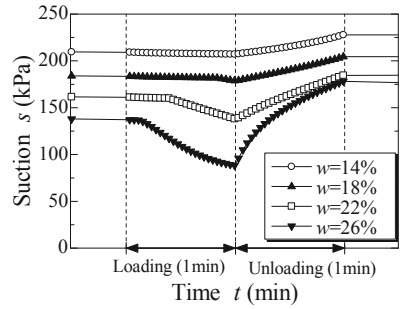

Figure 9. Changes in suction of element ○,3

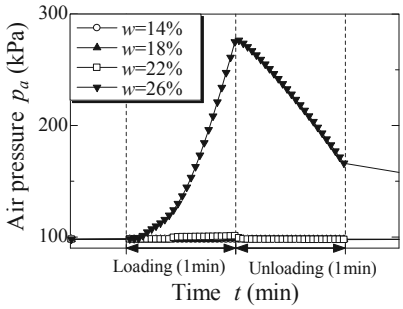

Figure 10. Changes in pore-air pressure of element ○,3

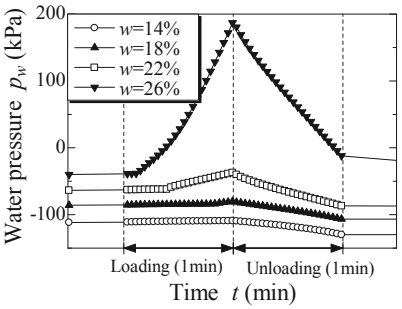

Figure 11. Changes in pore-water pressure of element ○,3

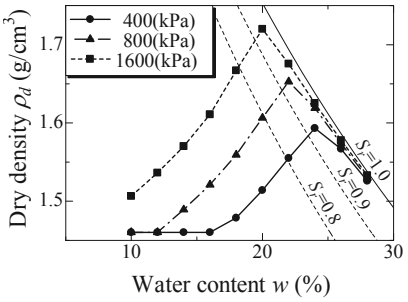

Figure 12. Water content - dry density relation

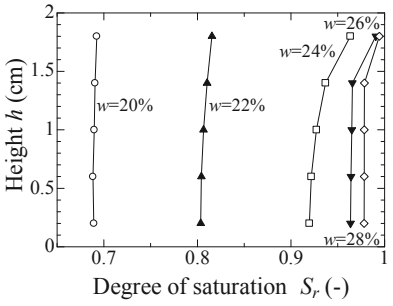

Figure 13. Distributions of saturation

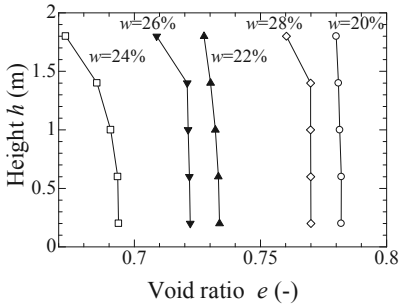

Figure 14. Distributions of void ratio

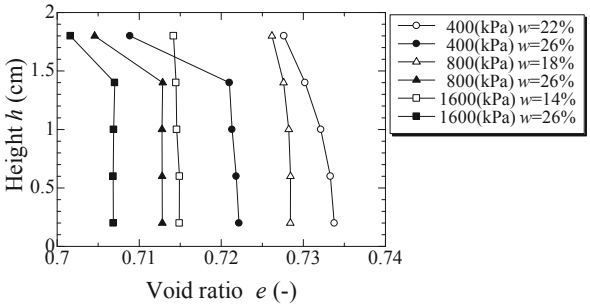

Figure 15. Distribution of void ratio on same dry density

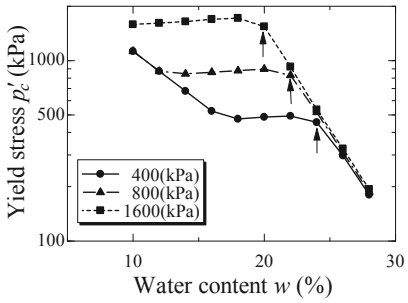

Figure 16. Water content – consolidation yield stress relation

The pore-air pressure of 98kPa indicates atmospheric pressure. Air permeability increases with decrease in the degree of saturation. Therefore, air can be drained easily on the specimen with lower moisture, while air pressure increases due to air entrapment on the specimen with higher moisture. Air pressure remains the same even after compaction due to drainage difficulty in the specimen with higher moisture. When air pressure change is fairly small, the suction change corresponds to the change in water pressure.

Figure 12 shows compaction curves, namely the relationship between water content and dry density obtained from static compaction simulations. This shows the maximum dry density at the optimum water content and the shapes agree with the actual compaction curve. The increase in maximum dry density and the decrease in the optimum water content with increase in the compaction load are expressed well here. Distributions for state quantities on the specimen compacted under 400kPa compaction load are introduced here. Figure 13 shows distributions for the degree of saturation after compaction. The specimen with higher moisture shows higher degree of saturation totally. Uniform distribution appears on the specimen with lower moisture. On the other hand, degree of saturation tends to increase gradually when it approaches the air-drained boundary. In the region over the optimum water content (about 24%), high degree of saturation appears only around the air-drained boundary since air permeability is fairly low. Figure 14 shows distributions of void ratio. There are different tendencies depending on whether it is under or above the optimum water

content, similar to degree of saturation. Permeability of compacted soil shown in Figure 1 is defined from stable flow on compacted soil under certain hydraulic gradient. Since lower permeability appears on the drier and denser specimen, the minimum permeability should appear under the optimum water content. However, the minimum permeability actually appears in the region over the optimum water content. It is assumed that this tendency can be attributed to distribution of degree of saturation and void ratio around the optimum water content shown in Figures 13 and 14. Figure 15 shows distribution of void ratio within the specimen compacted to dry density of around 1.55 (g/cm3). When we construct the embankment, dry density is specified for measurement standards after track maintenance work. However, from Figure 15 it is found that the distribution of void ratio varies according to compaction load and water content, even on the specimen with the same dry density.

Figure 16 shows the relationship between water content and yield stress of the compacted specimen in the unsaturated state, $p'_c = \zeta p'_{sat}$. Arrows in the figure indicate the optimum water contents of compaction curves. The yield stresses of the specimens compacted under 800 and 1600 (kPa) in the region with low-water content are overestimated due to characteristics of the constitutive model. Consequently, the peaks for yield stresses appear in the region that is little drier than the optimum water content (shown in Figure 19), and the simulation results agree with the experimental behavior.

4.2 *Simple shear simulation on compacted specimen*

Figure 17 shows the relationship between shear strain and shear strength on the specimen obtained from static compaction simulations in simple shear simulations. Figure 18 shows elastic shear modulus read from the specimen in Figure 17. The arrows in the figure indicate the optimum water contents of compaction curves where it is found that elastic shear modulus depends on dry density. However, the peaks of shear strength appear in the region that is little drier than the optimum water content (shown in Figure 19). This is attributed to the yield surface. Figure 20 shows the stress paths during shear. In the figure, the initial yield surfaces are drawn. The stress path reaches to the dry side of the yield surface first and is then bound for the critical state with strain softening. The size of the yield surface depends on plastic volumetric strain and degree of saturation. The former factor is related to dry density and the latter factor is related to water content. Additionally, the initial stress state after compaction depends on suction stress calculated with suction and degree of saturation shown in Eq.(2). Consequently, the maximum shear strength appears in the region that is drier than the optimum water content, as is generally known.

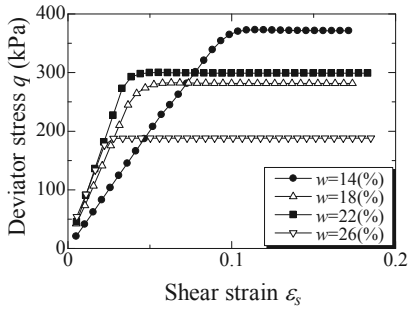

Figure 17. Strain-stress relationship on element ○,3 under shear

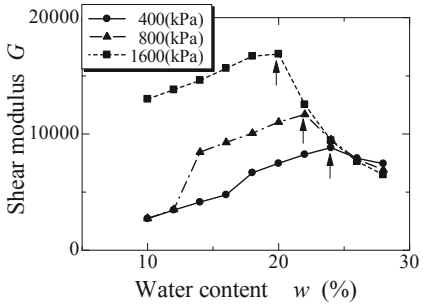

Figure 18. Water content and elastic shear modulus relationship

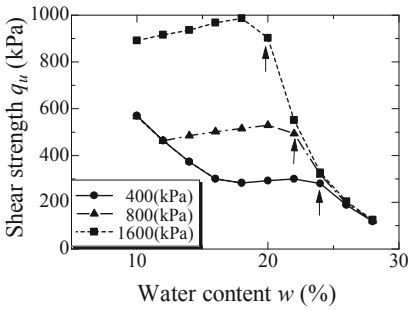

Figure 19. Water content and shear strength relationship

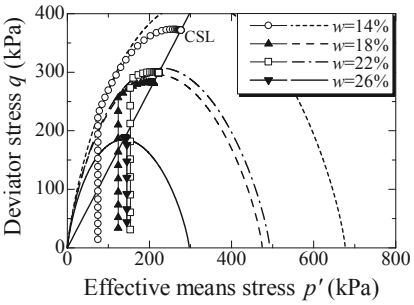

Figure 20. Stress paths of element ○,3

5 CONCLUSIONS

Static compaction and simple shear simulation were conducted with soil/water/air coupled F. E. analysis code, applying the constitutive model for unsaturated soil, DACSAR-MP. Consequently, the shape of the compaction curve and the characteristics of compacted soil could be reasonably expressed. This proves that 'compaction' can be defined by the initial and boundary condition problem on unsaturated soil.

6 REFERENCES

Borja R.I. 2004. A mathematical framework for three-phase deformation and strain localization analyses of partially saturated porous media. *Computer Methods in Applied Mechanics and Engineering* 193, 5301-5338.

Kawai K., Iizuka A., Hayakawa E. and Wang W. 2007. Non-uniform settlement of compacted earth structures caused by the deformation characteristics of unsaturated soil on wetting. *Soils and Foundations* 47(2), 195-206.

Kuno G. 1974. Soil compaction. *JSCE Magazine* 59(6), 18-22 (in Japanese).

Mualem Y. 1976. A new model for predicting the hydraulic conductivity of unsaturated porous media. *Water Resources Research* 12(3), 514-522.

Ohno S., Kawai K. and Tachibana S. 2007. Elasto-plastic constitutive model for unsaturated soil applied effective degree of saturation as a parameter expressing stiffness. *Journal of JSCE* 63(4), 1132-1141 (in Japanese).

Procter R. R. 1933. Four articles on the design and construction of rolled-earth dams. *Eng. News Record* 111, 245-248, 286-289, 348-351, 372-376.